Front. Phys. 13(2), 135201 (2018)
https://doi.org/10.1007/s11467-017-0735-1

RESEARCH ARTICLE

On the improvement of signal repeatability in laser-induced air plasmas

Shuai Zhang[1], Sahar Sheta[1,2], Zong-Yu Hou[1], Zhe Wang[1,†]

[1] *Department of Thermal Engineering, Tsinghua-BP Clean Energy Center, Tsinghua University, Beijing 100084, China*
[2] *National Institute of Laser Enhanced Science, Cairo University, Cairo 12613, Egypt*
Corresponding author. E-mail: †zhewang@tsinghua.edu.cn
Received July 20, 2017; accepted October 13, 2017

The relatively low repeatability of laser-induced breakdown spectroscopy (LIBS) severely hinders its wide commercialization. In the present work, we investigate the optimization of LIBS system for repeatability improvement for both signal generation (plasma evolution) and signal collection. Time-integrated spectra and images were obtained under different laser energies and focal lengths to investigate the optimum configuration for stable plasmas and repeatable signals. Using our experimental setup, the optimum conditions were found to be a laser energy of 250 mJ and a focus length of 100 mm. A stable and homogeneous plasma with the largest hot core area in the optimum condition yielded the most stable LIBS signal. Time-resolved images showed that the rebounding processes through the air plasma evolution caused the relative standard deviation (RSD) to increase with laser energies of > 250 mJ. In addition, the emission collection was improved by using a concave spherical mirror. The line intensities doubled as their RSDs decreased by approximately 25%. When the signal generation and collection were optimized simultaneously, the pulse-to-pulse RSDs were reduced to approximately 3% for O(I), N(I), and H(I) lines, which are better than the RSDs reported for solid samples and showed great potential for LIBS quantitative analysis by gasifying the solid or liquid samples.

Keywords laser-induced breakdown spectroscopy (LIBS), repeatability, air-plasma, signal fluctuations, plasma evolution

PACS numbers 42.62.Fi, 52.38.Dx, 52.50.Jm

1 Introduction

Laser-induced breakdown spectroscopy (LIBS) is a well-known atomic emission spectroscopy method that is receiving increasing attention from researchers and engineers worldwide [1–4]. In this technique, each species in the plasma emits its characteristic spectral radiation, which carries qualitative and quantitative information about the elemental composition of the material [5–8]. Over the last few decades, LIBS applications have covered a wide range of analytical demands, including industrial, medical, geological, agricultural, space-exploration, and environmental applications, with advantages of *in situ* and real-time analysis [9–14]. In most space-exploration and environmental applications, breakdown occurs in gas/air media. Laser-induced plasma (LIP) in ambient air is terse, and air can be considered as a homogeneous medium; thus, there is no non-stoichiometric ablation [15–17]. Nevertheless, the breakdown point of air is highly unstable, and the absorbed energy is fluctuant. Therefore, signal fluctuations in air plasmas are so strong that the quantitative determination performance is poor [18].

A headway in the control of the measurement stability and reproducibility of LIBS signals is one of the key actions towards the maturation of quantitative requirements. Quantitative LIBS analysis considers, with high precision and accuracy, the concentration of a species in a sample. The calibration curve of a reference sample is harshly affected by the analysis conditions. Consequently, the concentration determination of an unknown sample is extensively affected by the repeatability requirements [19, 20]. Day-to-day and pulse-to-pulse fluctuations of the plasma morphology in both the short and long terms influence the measurement stability. To obtain high analytical performance, the experimental settings should be optimized [21, 22]. In the literature, var-

ious methods have been proposed to improve the signal repeatability of plasma in LIBS. Double-pulse LIBS generally has a higher repeatability than single-pulse LIBS. Haider *et al.* compared single-pulse and double-pulse LIBS at different ambient pressures. At different pressures, DP-LIBS had a higher signal-to-noise (SNR) ratio and a lower relative standard deviation (RSD), yielding better repeatability [23]. The changes in the focusing parameters were also investigated to improve the repeatability of the LIBS signals. Tian *et al.* studied water plasmas at different focusing angles and concluded that larger focusing angles resulted in more focused and stabilized plasmas, yielding a lower RSD and improved repeatability of the plasma in bulk water [24]. For improving the repeatability on uneven surfaces, the effect of the change in the lens-to-sample distance has been frequently studied. Ashrafkhani *et al.* examined the change in the laser beam focusing position on samples with different degrees of evenness using an auto-focus system. The auto-focus system considerably decreased the standard deviation of the spectra [25]. Recently, Cortez *et al.* reported a simple device for improving the repeatability of LIBS signals by auto-focusing the lens-to-sample distance [26]. Chen *et al.* studied the energy absorption required for air plasma breakdown at different incident energies. The results showed that approximately 50% of the incident energy was absorbed when the input energy was slightly above the breakdown threshold range. The authors achieved repeatable plasma spectra and images up to a laser pulse energy of 80 mJ [27]. These studies show the work done under different experimental conditions and different methods to improve the repeatability of the LIBS spectra. Briefly, it is necessary to systematically study the effects of the focusing lengths and high laser-pulse energies on the plasma stability and LIBS signal repeatability.

In the present work, time-integrated spectra and real-time images of plasmas at various experimental settings (various laser energies and lenses focal lengths) were obtained to determine the optimum configuration for a stable plasma. The RSDs of line intensities and image pixels were calculated to track the repeatable signals. The laser-induced air plasma evolution through the optimum experimental conditions is presented via processes of breakdown, expanding, rebounding, squeezing, and vanishing of plasma. In addition, signal-collection enhancement is introduced via addition of a concave spherical mirror with an optical fiber.

2 Experimental

The LIBS experimental apparatus used in the current study is shown in Fig. 1. An air plasma plume was generated by employing a Q-switched Nd:YAG laser operating at the 1st harmonic wavelength: 1,064 nm. The pulse duration was 10 ns, the laser beam diameter was 8 mm, and the pulse repetition rate was 5 Hz. The fluctuation of the laser energy at 250 mJ was 1.86%, which was calculated using the RSD for 200 laser pulses. The divergence angle α of the laser was 0.6 mrad; thus, the minimum focus radius r was calculated to be 30 μm with a focusing lens having $f = 100$ mm ($r = f\alpha/2$). At the focus point, the average energy density was calculated to be 7.64×10^{10} W/cm^2. After the laser irradiation, plasma images were captured with an Andor Shamrock spectrograph (operating in the mirror mode) coupled with an Intensified Charge-Coupled Device (ICCD), Andor iStar 334i. A bi-convex lens with a focal length of 100 mm was used to collect the plasma emission at the camera entrance. In parallel, the plasma spectra were collected using an Avantes spectrometer (AvaSpec-Dual) coupled with a charge-coupled device having spectral ranges of 400–537 and 560–670 nm. The spectral signal was collected directly by an optical fiber, without a collimator, from the perpendicular direction to the laser incidence 10 mm away. The acceptance angle of the fiber was 15°; therefore, the fiber visual field was calculated to be ∼ 6 mm in diameter. This means that with the perfect alignment of the fiber, the whole plasma emission (in the line of fiber vision) should be collected efficiently. A special configuration was employed to study the signal enhancement using a concave spherical mirror in the face side of the fiber. The mirror was aligned to face the center of the plasma formation position. The spherical mirror used was aluminum-coated and had > 97% reflectance, a diameter of 80 mm, and a focal length of 100 mm.

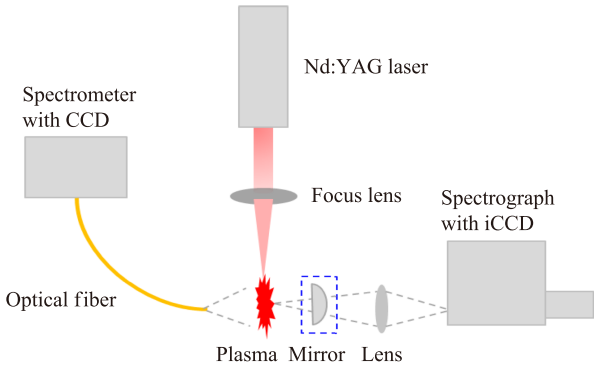

Fig. 1 Schematic of the LIBS experimental setup (the mirror in the dotted box was used specifically to study the signal-collection enhancement).

3 Results and discussion

The reproducibility of LIBS signals in a shot-to-shot basis is limited by the noise sources. Signal fluctuations are

mainly outlined from the trembling of laser pulses energies, laser-plasma interaction, shot noise, and instrumental (detector) thermal drift. In this study, the sources of the signal fluctuation were demonstrated from the plasma generation and collection. Two parameters of the plasma generation system — the laser pulse energy and the laser focusing — were varied in the experiment. The optimum configuration with the best repeatability results was selected. The plasma parameters, temperature, and electron density were studied in the optimum configuration. The signal collection was adjusted to compensate for the non-ideal plasma. It was enhanced through a rough comparison between the spectra obtained with and without a concave mirror. The backscattered collection of the emission plasma spectrum showed a higher time-integrated intensity than the spectrum collected without the mirror.

3.1 Repeatability of time-integrated plasma spectra

For LIBS spectra, the line intensities should have not only a high SNR but also good repeatability. The RSDs of the line intensities can show the amplitude of fluctuations and be used to compare the repeatability under various conditions. First, the pulse-to-pulse RSD of the one-line intensity with a certain setup is calculated. Then, RSDs of different lines within the same experimental parameters are averaged to represent the repeatability for that setup. In our experiment, the chosen spectral lines included N(I) 425 nm, O(I) 436 nm, H(I) 485 nm, O(I) 532 nm, O(I) 616 nm, O(I) 645 nm, N(I) 648 nm, and H(I) 656 nm. At different laser energies and focal lengths, the pulse-to-pulse RSDs of the line intensities were calculated among 200 laser shots. The delay time was 1 μs, and the integration time was 1 ms. The spectra repeatability at different laser energies and lens focal lengths were investigated to find the most suitable experimental adjustment. The average line intensities and pulse-to-pulse RSDs were calculated using raw data without normalization. The results shown in Fig. 2(a) reveal that the average line intensities correlate almost linearly with the laser energy. The plasma saturation regime appears with a flat-shape tendency at energies of > 250 mJ because of the complete ionization processes (optically thick plasma). In optically thick plasmas, highly dense ionized atoms are accumulated through the core area of the air inhomogeneous breakdown. Intense radiation trapping occurs, and the light emitted from the interior hot parts of the plasma travels to the outside cold regions. Consequently, the resultant spectrum in the spectrograph is weakened, and the linearity of the relationship between the intensity and the laser energy tends to saturate [28, 29].

On the other hand, as the laser energy is increased, the RSDs decrease and then increase. As the laser energy surpassed a certain value, the shot noise increased, according to Poisson distribution theory. The Poisson distribution is a discrete probability distribution that expresses the probability of a given number of events occurring in a fixed temporal or spatial scale. The shot noise or Poisson noise describes the fluctuations of the number of photons detected due to their occurrences being independent of each other. Fluctuations due to shot noise change with respect to the line intensity, according to the variance of the Poisson distribution [30]. The lowest RSD value was at $E \approx 250$ mJ. Regarding the effect of the focus length, Fig. 2(b) shows that the average line intensities decrease as the focal length increases, and the RSDs remain low when the focus length is < 100 mm but increase dramatically at focus lengths exceeding 100 mm. With the use of a shorter-focal length lens at a high energy, compact plasma in a smaller focal zone had higher line intensities. However, beyond a $\sim$ 100-mm focal length, the plasma length and size are attributed

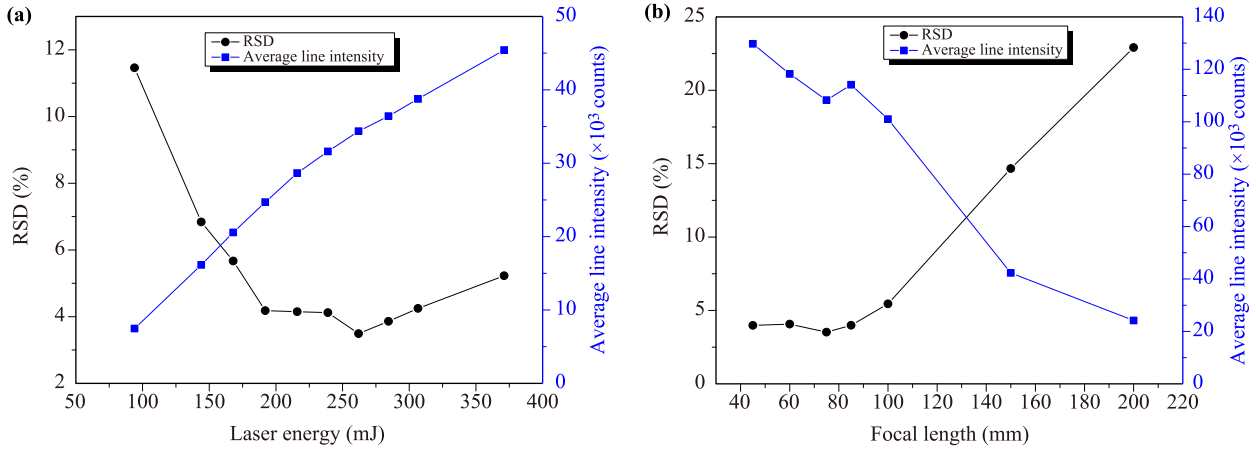

Fig. 2 RSDs and average line intensities for eight chosen lines at **(a)** different laser energies (focal length = 100 mm) and **(b)** different focal lengths (laser energy = 250 mJ).

to the highly fluctuating non-reproducible plasma with higher RSDs. Carranza *et al.* studied the single-shot spectra with different laser energies in the breakdown regime (185–350 mJ/pulse) of air plasma. Experiments suggested a saturation pulse energy of ∼ 255 mJ and a significant decrease of the RSD (using both the carbon peak/base and SNR values) at the same energy. The saturation was explained by the plasma absorption percentage of the incident laser energy after the breakdown. When a sufficient energy is deposited into the plasma and complete ionization occurs, the additional energy tends to expand the size of the plasma rather than increasing the temperature or the electron density [31]. Recently, Zuo *et al.* aimed to enlarge the interaction aperture of the plasma channel formed in air by adjusting the pulse energy, the focusing length, and the delay time. Different laser pulse energies (100, 150, 200, 250, and 300 mJ) with various delay times (30 and 60 ns) were studied. A homogenous plasma channel with a transverse diameter of approximately 0.8 mm was obtained in the case of a 250-mJ pulse energy and a delay time of 60 ns. A high-density, large-scale, and proper-gradient plasma channel with a total axial length of 2 mm was adjusted using a lens of $f = 100$ mm among three tested lenses (50, 100, and 150 mm) [32]. For improved repeatability, our results indicate optimum values of 250 mJ (pulse energy) and 100 mm (focal length), exhibiting a good agreement with the literature.

3.2 Plasma parameters study

The effects of different laser energies and focal lengths on the plasma temperature and electron density were investigated. The plasma temperature was calculated using the Boltzmann plot of the O lines at 436.825, 532.968, 615.818, and 645.598 nm, and the electron density was calculated using the H(I) 656.27 nm line. The results in Fig. 3(a) show that the plasma temperature and the electron density increased sharply as the laser energy increased and then reached a saturation level when the laser energy exceeded 200 mJ. When more energy was deposited into the plasma, saturation occurred, and size expansion was preferred instead of the plasma becoming hotter or denser. The plasma temperature and electron density showed no significant change with an increasing pulse energy. The approximate ranges of the plasma temperatures and electron densities were 6500–6900 K and (3–4) $\times 10^{17}$ cm^{-3}, with no statistical differences. Hereafter, the plasma parameters did not contribute directly to the high RSDs after the optimum repeatable pulse energy was observed. In Fig. 3(b), the temperature and the electron density decrease slightly for focal lengths of > 100 mm. The uncertainty of the determined plasma parameters was high; however, it appeared that a higher plasma temperature and electron density were required to improve the repeatability of the spectra. The RSDs are higher in the case of lower plasma temperatures and electron densities.

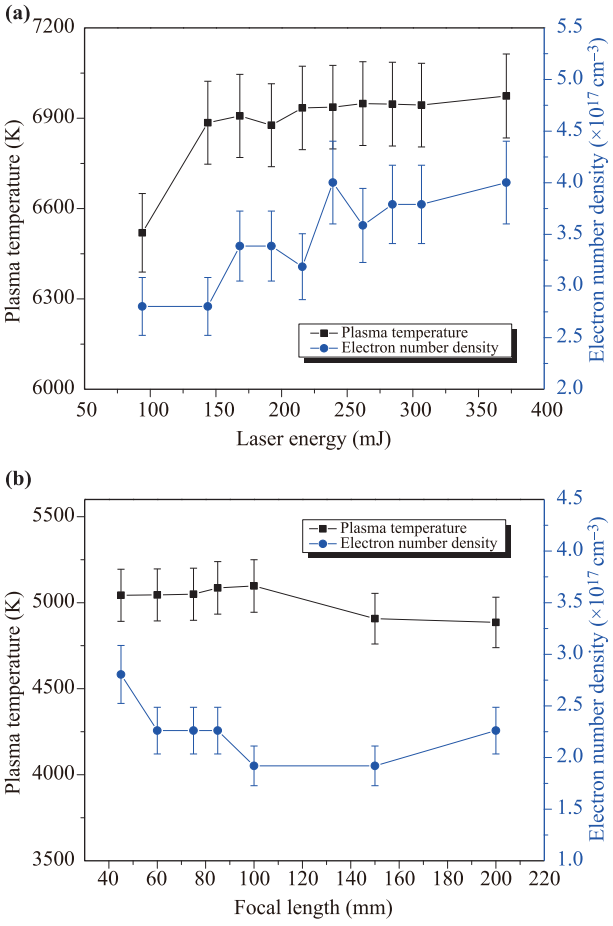

Fig. 3 Effects of the **(a)** laser energies and **(b)** lens focal lengths on the plasma temperature and electron number density.

3.3 Evolution of air plasma under optimum configuration

For a typical ns-LIBS, air breakdown begins with multi-photon ionization (bound-free transition), and then inverse bremsstrahlung (free–free transitions) dominates during the laser focusing on the air. The initial hot plasma expands into the cool surrounding air. The plume evolution is rapid in a direction opposite to the laser incidence. The backward plume component, which is close to the focusing lens, grows significantly faster than the slower component, which is closer to the focal spot [15]. Through the plasma evolution, the gas directly surrounding the plume is heated by the plasma radiation and becomes ionized. This ionization increases the evolution speed of the detached backward plume component.

The plasma plume expansion dynamics are strongly influenced by the incident laser pulse energy [33, 34]. In contrast to the plasma on the solid sample, the evolution of air plasma may include rebounding processes before vanishing. This rebounding occurs when the plume front reaches to the maximum displacement distance (lifetime depends on the incident laser deposited). If the air plasma bursts from a point, it expands isotropically into an ideal sphere. However, the air plasma is usually induced by the focal laser beam; thus, the initial plasma is a strip before expanding and grows in the direction of the incident laser. The absorption of laser radiation by the plasma accelerates the propagation towards the laser incidence direction and leads to anisotropic expansion of the plasma.

The plasma life-time includes the processes of breakdown, expanding, rebounding, squeezing, and vanishing. In Fig. 4, the air plasma evolution was investigated by capturing plasma images with different delay times (from 0–30 μs) under the optimum configuration ($E = 250$ mJ, $f = 100$ mm). The gate time was adjusted at 50 ns. Different attenuation plasma slices were used to obtain appropriate image intensities and protect the ICCD from intense light exposure. Each image was an average of 20 laser shots and was normalized to the maximum pixel intensity. The interval time of the laser pump switch and Q switch was 943 ns. From 943–955 ns, the laser interacted with air, and the interaction interface switched from the focus point to the laser incidence direction (red arrows pointing up). The plasma expansion was pear-shaped from 1–2 μs, owing to the initial plasma blast. From approximately 2–7 μs, the plasma continued its expansion but in a near-rectangular shape. This is attributed to the rebound processes of the momentum of the plasma or the internal shock waves. After 7 μs, the plasma was squeezed in a direction perpendicular to the laser incidence until approximately 18 μs and subsequently vanished.

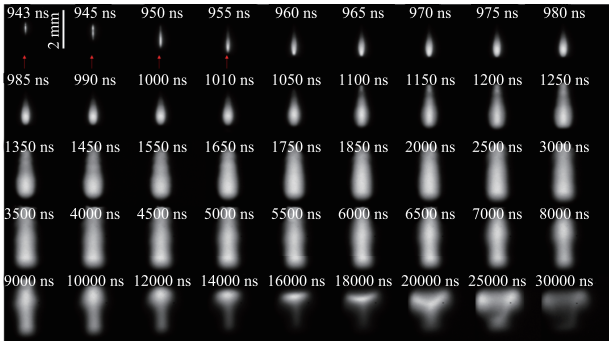

Fig. 4 Time-resolved images of the air plasma with different delay times starting from 943 ns (after Q-switch) at the optimum configuration ($E = 250$ mJ, $f = 100$ mm). Each image is the average of 20 acquisitions.

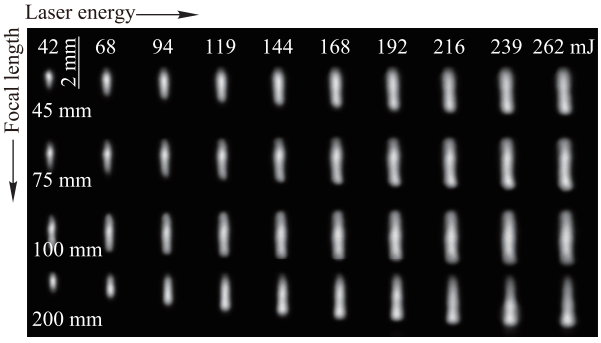

Fig. 5 Time-integrated images of laser-induced air plasma at various focus lengths and laser energies (laser incidence is bottom-up). Each image at a certain laser energy and certain focus length is the average of 10 laser shots performed under the same configuration. The ICCD was adjusted to a delay time of 1 μs and an integration time of 1 ms.

The plasma-evolution images indicate that the expanding and squeezing of the plasma contributed to its fluctuations and to the uncertainty of the signals. The early rebounding processes had a higher contribution to the fluctuations than other fluctuation sources through the plasma evolution. The rebounding and squeezing processes appeared to continue until the shock wave became weak. With the optimum setup, the plasma expanded from the initial strip of hot plasma and exhibited momentum rebounding, during which the plasma underwent good mixing that was beneficial to its plasma stability.

3.4 Time-integrated plasma images

Time-integrated plasma images were collected to demonstrate the formation of the most stable plasma. Using four different lenses ($f = 45$, 75, 100, and 200 mm) and 10 different laser energies ($E = 42$, 68, 94, 119, 144, 168, 192, 216, 239, and 262 mJ), each image was the average of 10 laser shots at the same laser energy and/or focal length. Each image is normalized to its maximum pixel intensity. Integrated plasma images are shown in Fig. 5, and the corresponding plasma lengths are plotted in Fig. 6. The plasma lengths were measured from the upper boundary to the lower boundary along the laser incidence direction using a plotting scale ruler. The laser-induced air plasma grew longer and wider as the laser energy increased and was maximized when the energy was > 250 mJ. With our setup, a laser energy of 250 mJ was the most suitable pulse energy for maintaining reduced RSD values. Regarding the focal lengths, according to Fig. 5, with a fixed laser energy, the plasmas formed at focus lengths of < 100 mm had better repeatability and size than those formed at > 100 mm. The optimum configuration of $E = 250$ mJ and $f = 100$ mm was confirmed

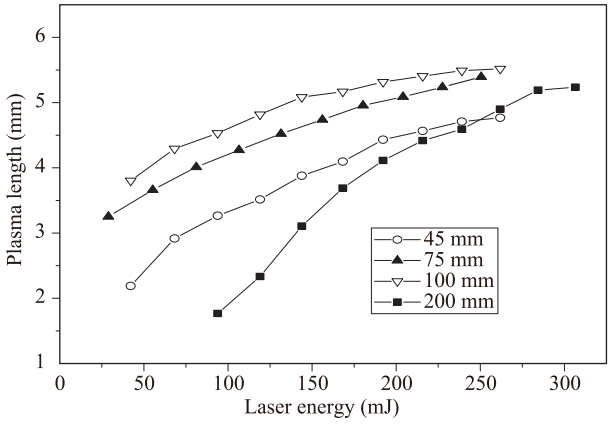

Fig. 6 Plasma lengths of time-integrated images at different laser energies and lens focal lengths.

by the integrated plasma images for the present experimental setup. The time-integrated morphology of the air plasma changed differently under various conditions. The air plasma evolution, the shock waves propagation, and the plasma shielding effects also changed with respect to the experimental parameters. With high laser energies, the shock waves moved faster, and the shielding effects were intensive.

3.5 RSDs for time-integrated plasma images

To further understand the effects of different focal lengths on the plasma evolution processes, time-integrated images of six different focal lengths (f = 45, 60, 75, 100, 150, and 200 mm) at a fixed laser energy of 250 mJ were investigated by calculating the RSDs of each pixel intensity. For each image, 200 laser shots were performed. Figure 7 clearly shows the core stable area of the plasma. Additionally, through the evolution, plasma splitting with the recorded intensity distribution can be observed. The RSD difference (i.e., fluctuations in the cooling process during expansion) through different parts of the plume is attributed to and strongly dependent on numerous variables, such as the air pressure, ablated air mass, and average charge state [35, 36]. At focal lengths of $<$ 100 mm, the overall distribution of the plasma evolution was stable and compact, except for an unstable interface part at the top. However, plasma formed by a lens with f = 100 mm had a concise base, with a stable homogeneous triangle distribution. At focal lengths of $>$ 100 mm, the plasmas had less concise bases, with inhomogeneous and unstable evolution.

3.6 Signal-collection enhancement

For the signal collection setup, a concave spherical mirror was used to enhance the collection efficiency of the plasma emission. Time-integrated spectra obtained with and without the mirror were compared to reveal the impact of the enhanced collection setup on the repeatability. The mirror was located on the opposite direction of the detection fiber, and the sphere center was coincident with the plasma, as shown in the Fig. 8 inset. The results show that the line intensities doubled with their RSDs reduced by approximately 25%. This is attributed to the anisotropy of the laser-induced plasma due to the enhancement of the fiber view field and collection. The plasma-evolution images and the pixel RSDs of the time-integrated plasma images shown in Figs. 4 and 5 clearly indicate that the plasma is an anisotropic source of the LIBS spectral signal. Increasing the solid angle of collection by introducing a concave spherical mirror is a suggestion for improving the signal repeatability.

4 Conclusion

The signal repeatability of LIBS plasma was investigated quantitatively, from the viewpoints of both signal generation and collection. Signal generation is a source of fluctuation that dominates the signal repeatability. For laser-induced air plasma, the signal generation is simple and is mainly affected by changes in the experimental setup, such as the laser energy and focus length. Additionally, the transient evolution of plasma contributes to the fluctuations from the signal generation. Furthermore, non-ideal generated plasma is inhomogeneous and anisotropic; thus, the signal collection must also be optimized. In this study, time-integrated spectra and images of laser-induced air plasma under various experimental configurations were studied to establish a stable plasma. The optimum configuration of E = 250 mJ and f = 100 mm exhibited best repeatability among the studied range of laser energies and lens focal lengths, which is attributed to the stable and homogeneous plasma with a compact base area. The air plasma evolution was investigated by capturing time-resolved images using ICCD.

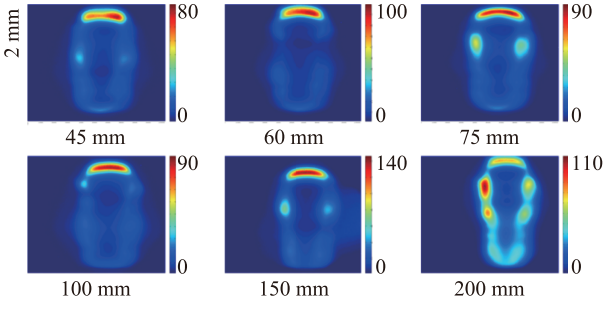

Fig. 7 RSDs of pixel intensities at different focus lengths (f = 45, 60, 75, 100, 150, and 200 mm) with a fixed laser energy of 250 mJ. The laser incidence is top-down. Each image represents 200 accumulated laser shots.

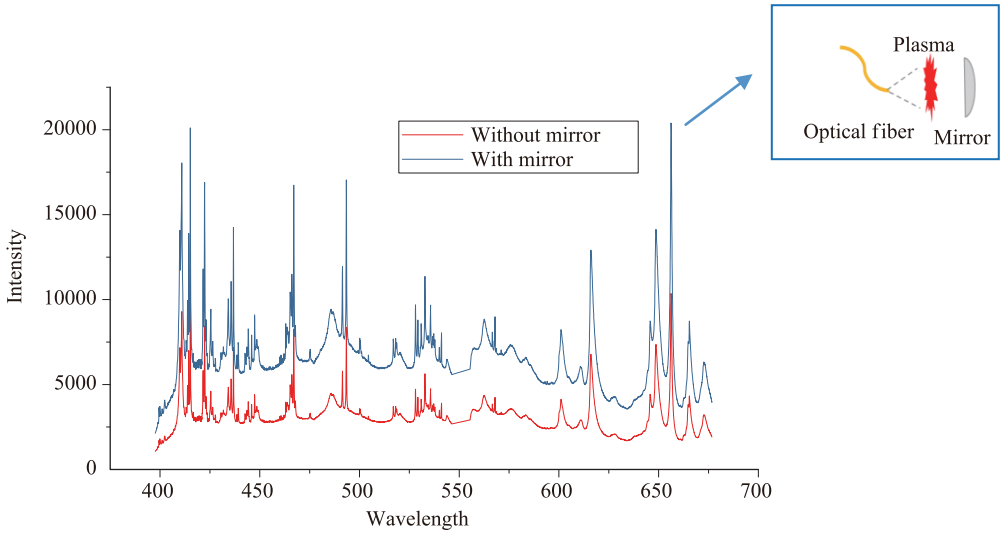

Fig. 8 LIBS integrated spectra of air plasma formed under the optimum configuration of $E = 250$ mJ and $f = 100$ mm with and without a concave mirror, used to study the signal-collection enhancement. The inset shows the configuration, where the mirror faces the optical fiber.

The violent rebounding processes of the plasma were reasons for the RSD increase at high laser energies. The signal collection was improved by using a concave spherical mirror to enhance the optical fiber collection. When the signal collection was optimized together with the signal generation, the improved repeatability of the laser-induced air plasma yielded a greater RSD enhancement than the solid samples, indicating that gaseous samples are alternatives for LIBS commercialization.

Acknowledgements The authors are grateful for financial support from the National Natural Science Foundation of China (Grant No. 61675110) and the National Basic Research Program of China (973 Program, Grant No. 2013CB228501).

References

1. J. P. Singh and S. N. Thakur, Laser-Induced Breakdown Spectroscopy, Amsterdam: Elsevier Science, 2007
2. A. Cremers and L. J. Radziemski, Handbook of Laser-Induced Breakdown Spectroscopy, USA: John Wiley & Sons, 2006
3. Z. Wang, T. B. Yuan, Z. Y. Hou, W. D. Zhou, J. D. Lu, H. B. Ding, and X. Y. Zeng, Laser-induced breakdown spectroscopy in China, *Front. Phys.* 9(4), 419 (2014)
4. Z. Z. Wang, Y. Deguchi, Z. Z. Zhang, Z. Wang, X. Y. Zeng, and J. J. Yan, Laser-induced breakdown spectroscopy in Asia, *Front. Phys.* 11(6), 114213 (2016)
5. H. R. Griem, Plasma Spectroscopy, New York: McGraw-Hill, 1964
6. D. W. Hahn and N. Omenetto, Laser-Induced Breakdown Spectroscopy (LIBS), Part I: Review of basic diagnostics and plasma-particle interactions: Still-challenging issues within the analytical plasma community, *Appl. Spec.* 64(12), 335A (2010)
7. D. N. Stratis, K. L. Eland, and S. M. Angel, Enhancement of aluminum, titanium, and iron in glass using pre-ablation spark dual-pulse LIBS, *Appl. Spec.* 54(12), 1719 (2000)
8. D. N. Stratis, K. L. Eland, and S. M. Angel, Dual-pulse LIBS using a pre-ablation spark for enhanced ablation and emission, *Appl. Spec.* 54(9), 1270 (2000)
9. R. Noll, C. F. Begemann, M. Brunk, S. Connemann, C. Meinhardt, M. Scharun, V. Sturm, J. Makowe, and C. Gehlen, Laser-induced breakdown spectroscopy expands into industrial applications, *Spectrochim. Acta B At. Spectrosc.* 93, 41 (2014)
10. A. K. Pathak, N. K. Rai, A. Singh, A. K. Rai, and P. K. Rai, Medical applications of laser induced breakdown spectroscopy, *J. Phys. Conf. Seri.* 548, 012007 (2014)
11. S. Qiao, Y. Ding, D. Tian, L. Yao, and G. Yang, A review of laser-induced breakdown spectroscopy for analysis of geological materials, *Appl. Spec. Revi.* 50(1), 1 (2015)
12. J. Peng, F. Liu, F. Zhou, K. Song, C. Zhang, L. Ye, and Y. He, Challenging applications for multi-element analysis by laser-induced breakdown spectroscopy in agriculture: A review, *Trends Analyt. Chem.* 85, 260 (2016)
13. A. K. Knight, N. L. Scherbarth, D. A. Cremers, and M. J. Ferris, Characterization of laser-induced breakdown spectroscopy (LIBS) for application to space exploration, *Appl. Spec.* 54(3), 331 (2000)
14. R. S. Harmon, R. E. Russo, and R. R. Hark, Applications of laser-induced breakdown spectroscopy for geochemical and environmental analysis: A comprehensive review, *Spectrochim. Acta B At. Spectrosc.* 87, 11 (2013)

15. A. De Giacomo and O. De Pascale, Laser induced plasma spectroscopy by air spark ablation, *Thin Solid Films* 453–454, 328 (2004)
16. N. Glumac and G. Elliott, The effect of ambient pressure on laser-induced plasmas in air, *Opt. Lasers Eng.* 45(1), 27 (2007)
17. A. Chen, Y. Jiang, H. Liu, M. Jin, and D. Ding, Plume splitting and rebounding in a high-intensity CO_2 laser induced air plasma, *Phys. Plasmas* 19(7), 073302 (2012)
18. Z. Wang, T. B. Yuan, S. L. Lui, Z. Y. Hou, X. W. Li, Z. Li, and W. D. Ni, Major elements analysis in bituminous coals under different ambient gases by laser-induced breakdown spectroscopy with PLS modeling, *Front. Phys.* 7(6), 708 (2012)
19. Z. Y. Hou, Z. Wang, J. M. Liu, W. D. Ni, and Z. Li, Signal quality improvement using cylindrical confinement for laser induced breakdown spectroscopy, *Opt. Express* 21(13), 15974 (2013)
20. H. Yin, Z. Hou, T. Yuan, Z. Wang, W. Ni, and Z. Li, Application of spatial confinement for gas analysis using laser-induced breakdown spectroscopy to improve signal stability, *J. Anal. At. Spectrom.* 30(4), 922 (2015)
21. V. Motto-Ros, E. Negre, F. Pelascini, G. Panczer, and J. Yu, Precise alignment of the collection fiber assisted by real-time plasma imaging in laser-induced breakdown spectroscopy, *Spectrochim. Acta B At. Spectrosc.* 92, 60 (2014)
22. E. Tognoni and G. Cristoforetti, Signal and noise in Laser Induced Breakdown Spectroscopy: An introductory review, *Opti. Lase. Tech.* 79, 164 (2016)
23. Z. Haider, Y. B. Munajat, R. Kamarulzaman, and N. Shahami, Comparison of single pulse and double simultaneous pulse laser induced breakdown spectroscopy, *Anal. Lett.* 48(2), 308 (2015)
24. T. Ye, B. Xue, J. Song, Y. Lu, and R. Zheng, Stabilization of laser-induced plasma in bulk water using large focusing angle, *Appl. Phys. Lett.* 109(6), 6 (2016)
25. B. Ashrafkhani, M. Bahreini, and S. H. Tavassoli, Repeatability improvement of laser-induced breakdown spectroscopy using an auto-focus system, *Opti. Spec.* 118(5), 841 (2015)
26. J. Cortez, B. B. Farias Filho, L. M. Fontes, C. Pasquini, I. M. Jr Raimundo, M. F. Pimentel, and F. de Souza Lins Borba, A simple device for lens-to-sample distance adjustment in laser-induced breakdown spectroscopy (LIBS), *Appl. Spec.* 71(4), 634 (2017)
27. Y. L. Chen, J. W. L. Lewis, and C. Parigger, Spatial and temporal profiles of pulsed laser-induced air plasma emissions, *J. Quant. Spectrosc. Radiat. Transf.* 67(2), 91 (2000)
28. H. Zwicker, Evaluation of plasma parameters in optically thick plasmas. Plasma Diagnostics, 1968
29. C. Aragón and J. Aguilera, CSigma graphs: A new approach for plasma characterization in laser-induced breakdown spectroscopy, *J. Quant. Spectrosc. Radiat. Transf.* 149, 90 (2014)
30. T. D. Arber, K. Bennett, C. S. Brady, A. Lawrence-Douglas, M. G. Ramsay, N. J. Sircombe, P. Gillies, R. G. Evans, H. Schmitz, A. R. Bell, and C. P. Ridgers, Contemporary particle-in-cell approach to laser-plasma modelling, *Plasma Phys. Contr. Fusion* 57(11), 113001 (2015)
31. J. E. Carranza and D. W. Hahn, Sampling statistics and considerations for single-shot analysis using laser-induced breakdown spectroscopy, *Spectrochim. Acta B At. Spectrosc.* 57(4), 779 (2002)
32. Y. Zuo, X. Wei, K. Zhou, X. Zeng, J. Su, Z. Jiao, N. Xie, and Z. Wu, Enhanced laser-induced plasma channels in air, *Chin. Phys. B* 25(3), 035203 (2016)
33. S. S. Harilal, Spatial and temporal evolution of argon sparks, *Appl. Opt.* 43(19), 3931 (2004)
34. S. S. Harilal, C. V. Bindhu, M. S. Tillack, F. Najmabadi, and A. C. Gaeris, Plume splitting and sharpening in laser-produced aluminium plasma, *J. Phys. D* 35(22), 2935 (2002)
35. S. Mahmood, R. S. Rawat, M. S. B. Darby, M. Zakaullah, S. V. Springham, T. L. Tan, and P. Lee, On the plume splitting of pulsed laser ablated Fe and Al plasmas, *Phys. Plasmas* 17(10), 103105 (2010)
36. P. Yeates and E. T. Kennedy, Spectroscopic diagnostics of plume rebound and shockwave dynamics of confined aluminum laser plasma plumes, *Phys. Plasmas* 18(6), 063106 (2011)